

Effect of Tool Pin Geometry and Process Parameters During FSW of Dissimilar Alloys of Mg

S. Yaknesh^{a*}, K. Sampathkumar^b, P. Sevel^c

^aTamilnadu College of Engineering, Department of Automobile Engineering, Palanisame Ravi Nagar, Karumathampatti, Tamil Nadu 641659, India.

^bKalaingar Karunanidhi Institute of Technology, Department of Mechanical Engineering, Pappampatti Rd, Pallapalayam, Kannampalayam, Tamil Nadu 641402, India.

^cS.A. Engineering College, Department of Mechanical Engineering, Chennai 600 077, Tamilnadu, India.

Received: September 30, 2021; Revised: December 15, 2021; Accepted: January 24, 2022

Effect of two distinctive tool designs along with other tool related parameters including speed of traverse of tool and offset distance of tool pin during friction stir welding of dissimilar AZ91C and AZ31B alloys of Mg were investigated. Experimental recordings revealed that all the joints fabricated during 1st set of investigations employing cylindrically tapered pin geometry and their offset distances being 0.5 mm or 1mm towards any one of the parent metals possessed flaws. Joint No: II-3 fabricated in 2nd set of investigations by employing 15mm diameter inner shoulder tool with threaded cylindrical tapered pin geometry at a tool offset distance of 0 mm was found to be free from flaws. This joint exhibited a tensile strength of 186 MPa which was 78.81% of AZ91C and 70.72% of another parent metal AZ31B. Existence of intermetallic phased constituents, namely, Mg₁₇Al₁₂ in several regions of fractured surfaces have contributed to the supplementary brittleness in the zone of nugget, and have reduced the tensile strength of the joint.

Keywords: Tool pin geometry, speed of tool traverse, tool offset distance, brittle fracture, AZ31B, AZ91C.

1. Introduction

Unique features of magnesium (Mg) and its alloys including excellent properties of damping, reasonable specific stiffness, larger specific strength, meager density etc., make them more preferable in automotive, marine, aerospace, biomedical and electronic industrial sectors¹⁻⁴. At the same time, alloys of Mg due to their certain elemental properties cannot be easily joined using the classical fusion-based welding methodologies^{5,6}. For example, the strong kinship of Mg alloys with nitrogen and oxygen, leads to the generation of magnesium oxide during joining. This magnesium oxide permanently remains in the area of the joint itself, as it cannot be cleared away easily, due to its large density and melting point features^{7,8}.

In addition to this, welding together dissimilar alloys of Mg and welding of alloys of Mg with other metals using classical techniques of joining is not an easy task, due to the alloy's inferior resistance towards corrosion and faster chemical reactivity⁹. Likewise, attempts to join alloys of Mg using larger input of heat energy will result in coarsening of grains in the seam of the joint, due to the alloy's larger thermal conductivity and low point of melting^{10,11}.

As per the perspective of metallurgy of joining, when compared with that of the classical techniques of joining, FSW (friction stir welding), a contemporary joining process, is competent enough to weld together alloys of Mg^{12,13}. This is because, FSW process joins Mg alloys before they reach

their point of melting, and hence, associated defects namely joint tumor, broader heat-affected region, etc., are curtailed^{14,15}. In addition to this, the temperature associated with FSW is much lesser when compared with that of the classical welding methodologies and this minimizes the after weld lacerations and residual stress formations. Another attractive characteristic that makes FSW more preferable for joining Mg alloys is the occurrence of dynamic recrystallization, which refines the microstructures completely, thereby, improving the performance of joints to a greater extent¹⁶⁻²⁰.

Many experimental investigations were carried out with respect to the joining of similar as well as dissimilar alloys of Al²¹⁻²⁶, similar as well as dissimilar of alloys Mg²⁷⁻³¹, etc. For example, Kumar et al.²⁴ employed the FSW process to join dissimilar alloys of aluminium namely AA6061 and AA5083 by using 3 distinctive pin-profiled tools together with variable speeds of traverse and rotation. During this process, AA6061 was kept on the side of retraction and AA5083 was kept on the side of advancement. Experimentation results conceded that the joints fabricated by taper threaded pin profiled tool at 40 mm/min and 900 rpm exhibited the largest tensile strength of 191.62 MPa.

An attempt was put forward by Baghdadi et al.²⁷ to enhance the mechanical related properties of friction stir welded alloy of Al–Mg–Si by means of post-joint treatment of heat and investigated the probability of regulating the growth of abnormal grain through distinctive parameters. In this attempt, joints were fabricated employing distinctive

*e-mail: yakneshsambath@gmail.com

speeds of travel and rotation and the welded samples were subjected to T6 category treatment of heat. Results revealed that, the precipitation relevant hardening particle's dissolution in the heat impacted region have reduced the strength of the welded samples.

FSW of dissimilar 6mm thick cast A390 and wrought AA6061 aluminium alloy flat plates were performed by Mahmoud Eskandari et al.²⁹. In this experimental work, the impacts of the location of the alloy material, speeds of traverse, and rotation were taken into account for investigating the features arising w.r.t microstructure and thermomechanical aspects, by formulating a 3-dimensional FEM (finite element method). It was recorded that, when cast alloy A390 was placed on the side of retraction and advancement, the linear to rotational speed ratios contributing for the high-quality weld was 250–120 rev/cm and 250–200 rev/cm respectively. The weld samples attained by placing cast alloy A390 on the side of advancement exhibited unique atomic diffusion and enhanced mixing of parent materials.

Wen Wang et al.³¹ experimentally studied the impact of the rate of rotation of the fatigue cycle during FSW of AZ31 alloy of Mg. It was observed that the impact of the rate of rotation was significant on the size of the grains of the attained joints, but negligible on the grain textures present in the region affected by thermal-mechanical aspects and in the zone of nugget. Fabricated AZ31 joints demonstrated a symmetrical hysteresis loop irrespective of the rate of rotation. Joint fabricated at 950 rpm possessing fine-sized structural grains demonstrated very larger amplitude of stress when compared with that of the joint fabricated at 1500 rpm having coarse-sized structural grains.

In recent years, researchers have also flourishingly employed FSW to join alloys of Mg with other metals including Steel, Ti, Al³²⁻³⁸, etc. For instance, Md and Birru³³ investigated the mixing of materials during FSW of aluminium alloy (namely AA6082-T6) and magnesium alloy (namely AZ91), by changing the position of these two distinctive parent materials on the side of advancement and retraction alternatively. It was observed that, during the placing of AZ91 on the side of advancement, a higher volume of aluminium was soluble in the region of nugget, when compared with that of the placing of AZ91 on the side of retraction. Likewise, the largest value of the mechanical strength of nearly 172 MPa was exhibited by the joint having Mg as its side of advancement and the lowest value of nearly 156 MPa was exhibited by the joint having Mg as its side of retreatment.

Baghdadi et al.³⁶ made an attempt to join dissimilar Al-Mg alloys using FSW by employing distinctive conditions of offset of tool, speeds of travel and rotation. Flaw free joints with superior strength were attained during the employment of intermediary speed of rotation, lower tool travel and when the pin is inserted at the middle of the line of weld. When the pin of the tool was inserted at an offset of +1mm or -1mm, joints possessing flaws (including cracks, tunnels, pores etc.,) were attained.

An experimental attempt to friction stir butt weld low carbon steel (Q235 grade) and magnesium alloy (AZ31B) was made by Yongsheng Meng et al.³⁸ using a tool possessing cone-shaped truncated threaded pin. It was experimentally

proven that, the tool with truncated threaded pin had improvised the fluidity of steel to a greater extent and has also enhanced the reaction of the interface between the alloy of steel and magnesium. The dissimilar joint of Q235 grade low carbon steel and AZ31B Mg alloy fabricated at 850 rpm and 75mm/min exhibited the largest value of mechanical strength of nearly 190 MPa, which is about 75% of the strength of the Mg parent metal.

From the above-detailed literature, it can be observed that most of these FSW-based experimental works have been carried out w.r.t joining of similar alloys of Mg and joining of Mg alloys with other metals (namely Al, Steel, Ti, etc.). The research works focusing on the FSW of dissimilar alloys of Mg is quite limited. Hence, there exists a vital need for carrying experimental researches on the joining of dissimilar alloys of Mg using the FSW process. Moreover, in order to gain more understanding of the weldability of alloys of Mg and to broaden the usage of alloys of Mg in several industrial sectors including automotive and aerospace, it is of great prerequisite and priority to perform experimental attempts to join dissimilar alloys using the FSW process. In addition to this, the impact of the tool offset distance during FSW of dissimilar alloys of Mg have not been investigated to greater extent and there exists a need for understanding its impact on the properties of the fabricated joints. As a result, in this investigational work, an experimental effort was put forward to join two distinctive alloys of Mg namely AZ31B and AZ91C by friction stir welding and to gain more understanding about the impact of several parameters of the FSW process by employing tools with two distinctive pin geometries under varying parameters of speeds of traverse of the tool, tool offset distance.

2. Methodology of Research

AZ31B and AZ91C alloys of Mg in the form of rectangular plates were taken as the material of investigation. These rectangular plates possessed a width of 55mm for a length of 100 mm and together with a thickness of 6mm. The chemical composition of the materials of investigation is described in Table 1.

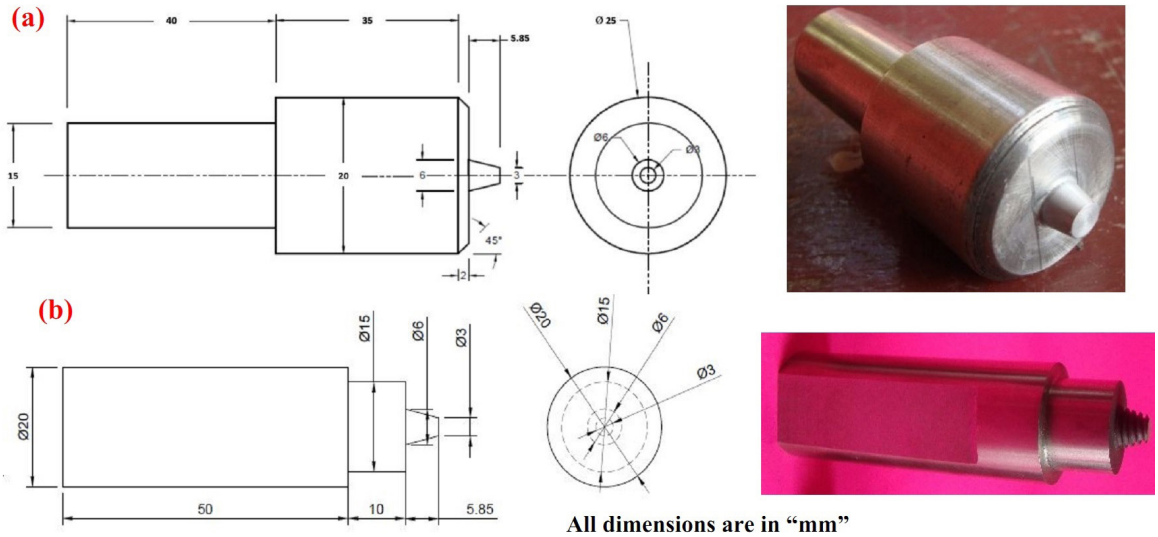
AZ31B rectangular plate was placed on the side of advancement and AZ91C plate was placed on the side of retraction throughout the entire investigation. 2 completely distinctive sets of the investigation were carried out by employing tools with 2 distinctive pin and shoulder geometries (namely tool I & tool II). Both the tools were fabricated out of M42 grade high-speed steel material.

The diagrammatic representations of the various views (front, side and isometric view) of the employed tools with 2 distinctive geometries (tool I & tool II) are illustrated in Figure 1a & b. As seen in Figure 1a, the tool I has a cylindrically tapered pin for a 5.85 mm length, with a 15 mm diameter outer shoulder for a length of 40 mm and a 20 mm diameter inner shoulder for a length of 35mm. Likewise, as seen in Figure 1b, tool II has a threaded cylindrically tapered pin for a 5.85 mm length, with a 20 mm diameter outer shoulder for a length of 50 mm and a 15mm diameter inner shoulder for a length of 15mm.

1st set of investigations were carried out by employing tool I and 5 joints were fabricated by placing the tool pin at

Table 1. Constituents of the materials being investigated in this work.

Material	Mn	Si	Zn	Ni	Fe	Cu	Al	Mg	Tensile Strength	Yield Strength	% of elongation
AZ31B	0.31	0.079	0.85	0.0049	0.005	0.051	3.15	Balance	263 MPa	178 MPa	11.7%
AZ91C	0.30	0.12	0.73	0.01	0.01	0.08	9.13	Balance	236 MPa	130 MPa	7.7%

**Figure 1.** Illustration of the tools employed with 2 distinctive geometries: (a) Tool I with cylindrically tapered pin geometry and (b) Tool II.

different distances from the center of the line of joint. During the 1st set of investigations, the other parameters namely speed of tool rotation (1000 rpm), speed of tool traverse (2 mm/sec), axial force (5kN) and angle of tilt (0.5°) were maintained at constant values. During 2nd set of investigations, tool II was employed to fabricate joints of dissimilar alloys of Mg and a total of 5 joints were fabricated in this set by employing 5 different speeds of tool traverse including 0.5 mm/sec, 1.0 mm/sec, 1.5 mm/sec, 2.0 mm/sec and 2.5 mm/sec. In this 2nd set of investigation, the other parameters namely speed of tool rotation (850 rpm), axial force (3.5 kN), angle of tilt (0°) and tool offset distance (0 mm) were maintained at constant values. Table 2 describes in detail, the combination of the parameters employed in this investigation.

3. Results and Discussions

3.1. Investigations on Tool I: Structural appearances

Structural appearances of the distinctive AZ91C and AZ31B Mg alloy joints fabricated by Tool I are portrayed in Table 3. From this table, it can be understood that the surfaces of the distinctive joints of alloys of Mg fabricated at tool offset distances of 0.5 mm and 1.0 mm both towards the AZ31B side and AZ91C side were found to possess some surface irregularities. For example, we can observe the presence of uneven, hard weld surfaces in Joint No: I-1, which reveals us the fact that the insertion of tool pin at a distance 0.5 mm from the line of joint towards the side of AZ31B have resulted in the creation of hindrances which

have impeded the smooth rotation of the tool shoulder during its course of travel.

Likewise, the insertion of the tool pin profile at a distance of 1.0 mm away from the line of joint towards the side of AZ91C had resulted in the generation of unwelded portions towards the end of the joint area in Joint No: I-4. As the tool pin have moved towards the side of AZ91C, the flow of material towards the side of AZ31B demanded a higher volume of input of heat for facilitating the uniform material flow and as this required heat cannot be generated, it had led to the improper weld portions as observed in Table 3^{20,25}. At the same time, the surface of the Joint No: I-3 (fabricated by maintaining 0mm tool offset distance, i.e., the tool pin was inserted exactly in the line of joint) seems to be smooth and glossy without any irregular or uneven portions, when compared with other joint surfaces. This is very much similar to the results recorded by Baghdadi et al.³⁶ during their investigation in joining dissimilar Al-Mg alloys by employing distinctive conditions of offset of tool, namely -1mm, 0mm and 1mm offset. It was recorded in this investigation that, the flaw free joints with superior strength were attained during the employment of intermediary speed of rotation, lower tool travel and when the pin is inserted at the middle of the line of weld, i.e., at 0mm tool offset distance.

3.2. Investigations of macro and micro-structures

In order to acquire more knowledge on the quality of the distinctive AZ31B and AZ91C joints of alloys of Mg fabricated by employing different tool pin offset distances, examinations of the macro and micro-structures were carried out and the attained observations are tabulated in

Table 2. Description of the combination of parameters adopted during the 2 experimental sets.

Tool offset distance from the line of joint	1 st set of Investigations using Tool I				2 nd set of Investigations using Tool II				
	Speed of tool rotation (rpm)	Speed of tool traverse (mm/sec)	Axial force (kN)	Angle of tilt (degree)	Tool offset distance from the line of joint	Speed of tool rotation (rpm)	Speed of tool traverse (mm/sec)	Axial force (kN)	Angle of tilt (degree)
0.5 mm towards AZ31B side	1000	2	5	0.5 ^o	0 mm	850	0.5	3.5	0 ^o
1.0 mm towards AZ31B side	1000	2	5	0.5 ^o	0 mm	850	1.0	3.5	0 ^o
0 mm (matching with line of joint)	1000	2	5	0.5 ^o	0 mm	850	1.5	3.5	0 ^o
1.0 mm towards AZ91C side	1000	2	5	0.5 ^o	0 mm	850	2.0	3.5	0 ^o
0.5 mm towards AZ91C side	1000	2	5	0.5 ^o	0 mm	850	2.5	3.5	0 ^o

Table 3. Structural appearances of the distinctive AZ91C and AZ31B Mg alloy joints fabricated by Tool I.






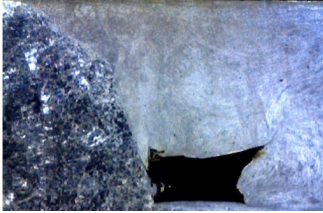
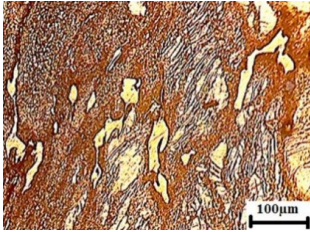
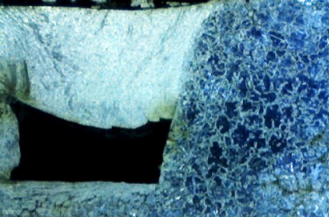
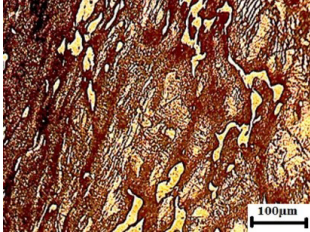
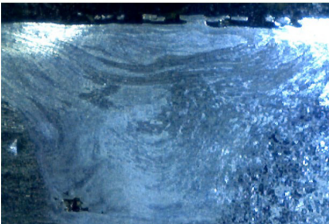
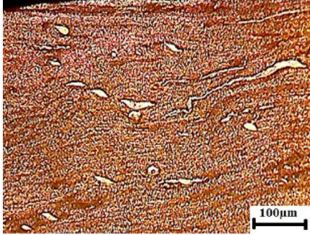
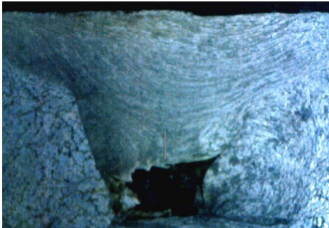
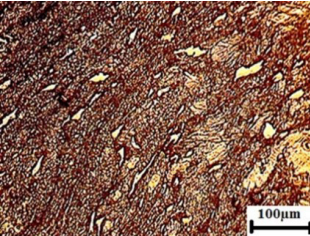
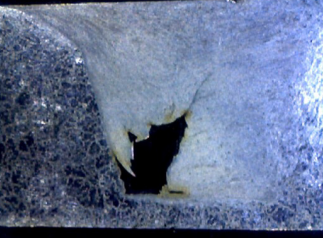
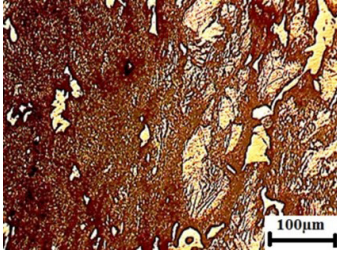
Joint No	Tool offset distance from line of joint & other employed parameters	Structural appearances of the distinctive AZ91C and AZ31B Mg alloy joints fabricated by Tool I	Inferences from the structural appearances of the fabricated distinctive joints
I-1	Tool pin 0.5 mm towards AZ31B side; 1000 rpm; 2mm/sec; 5 kN; 0.5 ^o		Uneven, hard weld surfaces revealing the difficulty experienced by tool shoulder in penetrating the joint areas
I-2	Tool pin 1.0 mm towards AZ31B side; 1000 rpm; 2mm/sec; 5 kN; 0.5 ^o		Coarse & irregular weld surfaces on one side of joint revealing the lack of experience of sufficient amount of heat on that side
I-3	Tool pin 0 mm (exactly at line of joint); 1000 rpm; 2mm/sec; 5 kN; 0.5 ^o		Presence of smooth surfaces over the majority regions along the area of joint
I-4	Tool pin 1.0 mm towards AZ91C side; 1000 rpm; 2mm/sec; 5 kN; 0.5 ^o		Unwelded portions at the end of the area of joint revealing the hinderances being created against the flow of material from one side to another side
I-5	Tool pin 0.5 mm towards AZ91C side; 1000 rpm; 2mm/sec; 5 kN; 0.5 ^o		Wobbly weld surfaces for longer areas revealing the difficulty experienced by tool shoulder in penetrating the joint areas

Table 4. It can be seen that, the macro-structures of the joints designated as I-1, I-2, I-4 and I-5 were found to be present with flaws such as tunnels, large-sized voids, etc at their root (bottom) portion. This concedes us the fact, the employment of tool pin offset distance either towards the

side of advancement or towards the side of retraction had deteriorated the quality of the joints^{19,28}.

At the same time, the I-3 joint possesses small-sized voids when compared with that of the remaining four joints. This strengthens the recorded data that, during the joining

Table 4. Macro and Micro- structures of distinctive AZ31B and AZ91C joints of alloys of Mg fabricated at different tool pin offset distances.

Joint No	Macro-structure	Micro-structure at the zone of nugget
I-1		 Grain Size: 28.2 μm
I-2		 Grain Size: 26.5 μm
I-3		 Grain Size: 14.7 μm
I-4		 Grain Size: 20.1 μm
I-5		 Grain Size: 27.8 μm

of distinctive alloys by FSW, tool pin offset distance should be maintained at 0mm, i.e., the tool pin should be inserted exactly on the line of joint.

Further investigations on the microstructure of the zone of nugget of these fabricated distinctive joints of alloys of Mg, it can be seen that, mixing of particles and fragmentation of grains have not occurred in the zone of nugget of I-1, I-2, I-4 and I-5 joints. Even though, tool offset distance of 0mm was adopted during fabrication of the I-3 joint, it can be observed that, the fragmentation of grains have not taken place in an appreciable manner and the parallel layers of unequally plasticized grains reveal us that, the grain fragments

have experienced surplus volume of heat and stress due to the large diameter of tool shoulder.

Moreover, we can observe voids (either larger or smaller) in all the fabricated joints, irrespective of the adopted tool offset distance, which helps us to interpret that, the employed tool pin geometry namely cylindrically tapered pin had not generated uniform scratching of the grain particles from the root portion and have led to these voids. This is very much similar to the experimental results recorded by Patel et al.³⁰, which states that, the taper cylindrical tool with an 18mm shoulder diameter was not capable enough to fabricate joints without flaws. This investigation registered that, the cracks

were obtained in the upper region of the weld portion and voids in their interior region, due to the insufficient volume of generation of heat by the employed taper cylindrical tool. At the same time, it should be noted that, the tool offset distance of 0mm seems to be more appropriate when compared with that of the remaining adopted tool offset values. Yet, a minimal volume of the void can be observed at the root portion of the fabricated joint, it could have resulted due to the disparity in the combination of other parameters being employed in this 1st set of experimentation.

3.3. Investigations with tool II

As the employed geometry of cylindrically tapered pin had not generated flawless joints, it was decided to modify the design of the employed tool by including threads in its pin geometry, i.e., a tool with cylindrically tapered threaded pin profile in the 2nd set of experimental investigations. Based on the above-recorded observations, it was also decided to reduce the diameter of the inner shoulder of the employed tool by 5mm, i.e., a 15 mm diameter inner shoulder as seen in Figure 1b. This reduction in diameter of tool shoulder was adopted with the objective of generating the ideal volume of heat, as the previously employed tool shoulder diameter (20 mm) had generated surplus volume of heat, leading to attainment of parallel layers of unequally plasticized grains in the zone of nugget.

In addition to these changes, 2nd set of experimental investigation was carried out at 5 distinctive speeds of tool traverse including 0.5 mm/sec, 1.0 mm/sec, 1.5 mm/sec, 2.0 mm/sec and 2.5 mm/sec, with other parameters i.e., speed of rotation of the tool (850 rpm), force welded from upwards (3.5 kN), the tilt angle of employed tool (0°) and offset distance of tool (0 mm) being maintained at fixed levels. Table 5 illustrates in detail, the structural appearance and macro-structure of the distinctive AZ31B and AZ91C joints of alloys of Mg being fabricated as a part of the 2nd set of experimental investigations.

From this Table 5, it can be seen that the appearance of the surfaces of these distinctive Mg alloy joints had improved to some reasonable extent when compared with that of the 1st of experimental investigations. A close observation of the macro-structures of these joints concedes us that, the change of the pin geometry of the employed tool (from tool I to tool II) had resulted in an appreciable change in the level of penetration as well as in the appropriate mixing of the constituents of parent metal in all the fabricated joints. It can be noticed that, the joints with joint nos II-1, II-2, II-4 and II-5 possess defects including pores, cavities, voids etc. The intensities of these defects can be observed to increase with the employment of higher speeds of tool travel (namely 2.0 mm/sec and 2.5 mm/sec). This is because, escalation in the speed of traverse of the tool reduces the volume of heat being generated and had led to a magnified volume of flaws in II-4 and II-5 joints.

At the same time, the employed lower speeds of tool traverse (namely 0.5 and 1.0 mm/sec) were not rapid enough to transfer the generated heat to the entire regions of the joint area, especially from root to crest of the joint area^{18,28,39}. As a result, the joints fabricated at lower speeds of tool traverse (II-1 and II-2) possess flaws in their bottom-most portions,

while the remaining portions (i.e., crest and middle portions) had experienced proper mixing of materials.

It was proved by Kumar et al.²⁴ that, the action of the course of the grains inside the welded specimen was equiaxed & appreciable and the thrust temperature together with extensive plastic reformation due to the mixing action of the taper tool with threaded structures have reduced the size of the grains significantly in the welded specimen. In similar manner, by carefully investigating the macrostructure of the flawless joint fabricated at 1.5 mm/sec tool traverse speed, we can interpret that, the employed pin geometry (namely threaded cylindrically tapered pin) of the tool had performed the function of enabling the mixture of constituents of the distinctive parent metals from root portion to crest portion in an enhanced manner^{22,40}. In addition to the pin geometry, the employed and modified inner shoulder diameter (of 15mm) of the tool have also played a significant role in exerting the required amount of force axially over the entire region of the joint.

3.4. Investigations on Joint No:II-3

Figure 2. portrays the photograph of some of the dissimilar FSWed AZ91C and AZ31B joint configuration fabricated during the 2 experimental sets. In the 2nd set of experimental investigations, as the macro-structure of the joint (with Joint no II-3) fabricated at a speed of traverse of 1.5 mm/sec is completely free from all forms of flaws, micro-structural investigation of the several zones of that joint will help us to acquire a better understanding on the impact of the employed parameters.


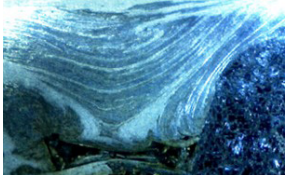

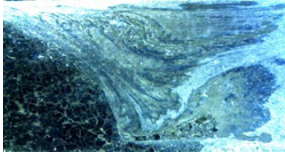

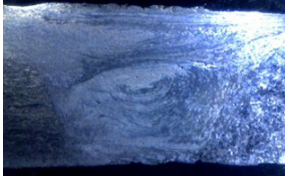

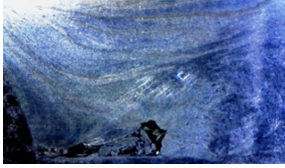
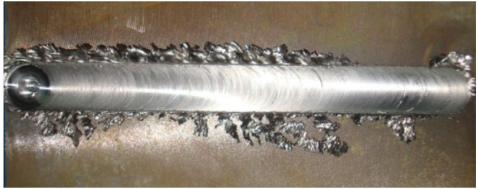
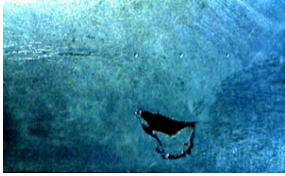
The cross section of the weld bead of this defect free joint is illustrated in the Figure 3. In this Figure 3, the several regions of the friction stir welded joint, namely Nugget weld (NW, i.e., zone of nugget), thermo mechanically affected zone (TMAZ) and heat affected zone (HAZ) are marked clearly, such that each zone can be identified easily.

Figure 4a & b illustrate the micro-structural image of the parent metals AZ91C and AZ31B respectively. It can be observed from Figure 4a that, the parent metal (AZ91C) possesses a dendrite type of structure in which, the huge grains of Mg-based solid solution with large precipitates of Mg₁₇Al₁₂ are visible at the boundaries of grains. The average size of the grains in this parent metal (AZ91C) is 38.9 μm. Likewise, the other parent metal (AZ31B) as seen in Figure 4b possesses parallel flowing grain structures containing partially dissolved precipitates of Mg₁₇Al₁₂. The average size of the grains in this parent metal (AZ31B) is 21.4 μm.

The region of the interface of the parent metal with the thermo-mechanically influenced region is illustrated in Figure 4c. In this region, it can be seen that, the fine flow of the fragmented constituents had occurred, due to the combined impact of the employed tool pin geometry (threaded and tapered pin geometry) and the ideal speed of tool traverse (1.5 mm/sec)^{7,37,41}. The fragmented constituents have also experienced partial re-crystallization during their flow to other side of the parent metal.

Figure 4d illustrates the region influenced by the inner diameter of the tool shoulder. Employment of suitable shoulder diameter (15mm) and pin geometry together with ideal traverse speed have enabled the generation of required

Table 5. Structural appearances and macro-structure of the distinctive AZ91C and AZ31B Mg alloy joints fabricated by Tool II.

Joint No	Speed of traverse of employed tool	Structural appearances of the distinctive AZ91C and AZ31B Mg alloy joints fabricated by Tool II	Macro-structure of the joints fabricated by Tool II	Grain Size and Inferences
II-1	0.5 mm/sec			Grain Size: 15.8 μm . Tunnel defects at the bottom portion
II-2	1.0 mm/sec			Grain Size: 14.6 μm . Minute pores at the bottom portion
II-3	1.5 mm/sec			Grain Size: 10.2 μm . Joint Surface free from flaws
II-4	2.0 mm/sec			Grain Size: 16.7 μm . Cavities at the bottom portion
II-5	2.5 mm/sec			Grain Size: 17.9 μm . Pores at the bottom portion

volume of heat, suitable enough to plastically deform the constituents of both the parent metals. Thermo-mechanically influenced region together with the constituents of the parent metal (AZ31B) can be seen in Figure 4e. It can be seen that the grain fragments of AZ31B have experienced enough volume of heat and stress and are directed towards the side of retraction. From Figure 4f, we can visualize, the rapid and uniform mixing of the completely re-crystallized grain constituents of AZ31B with the constituents of the AZ91C, being impacted by the turbulent action of tool pin geometry and tool shoulder.

In Figure 4g portrays a region where the interface of the constituents of AZ31B are getting interfaced in the zone of

nugget, which contains ultra-fine fragmented particles and constituents of both the parent metals (namely AZ31B and AZ91C). Centre of the zone of nugget of the fabricated distinctive joint of alloys of Mg is seen in Figure 4h and the size of the grains in this zone is 10.2 μm . It can be seen that this zone contains completely well-refined grains structures of solid solution of Mg and entirely dissolved phases of several constituents of both the parent metals.

With the objective of justifying the above mentioned fact, that the constituents of both the parent metals are present in the zone of nugget, the images and constituent element graphs generated during the analysis carried out using energy dispersive X-ray (EDAX) are illustrated in



Figure 2. Photograph of some of the dissimilar FSWed AZ91C and AZ31B joint configuration fabricated during the 2 experimental sets.

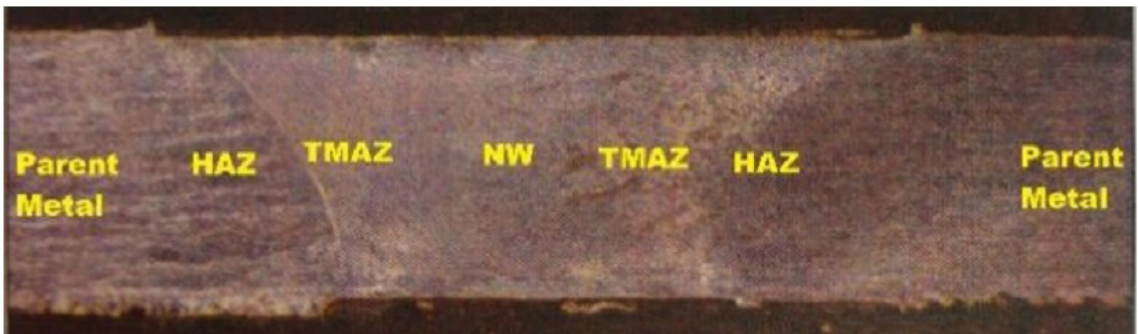


Figure 3. Cross sectional illustration of the defect free friction stir welded joint (i.e., Joint No: II – 3).

the Figure 5a-c. Figure 5a and b portrays the EDAX image and elemental graphs of the parent metals, i.e., AZ91C and AZ31B respectively.

Figure 5c portrays the EDAX image and elemental graphs of the zone of nugget of the flaw free joint No: II – 3 and from this images, it can be understood that, in the zone of nugget of this joint No: II – 3, the constituents of the parent metals (AZ91C and AZ31B) have dissolved with one another completely and the grains have fragmented, due to the impact of the dynamic recrystallization.

It must be noted that, only the speed of tool traverse of 1.5mm/sec had yielded a joint, being entirely free from flaws. Employment of other ranges of speeds of tool traverse

(including 0.5, 1.0, 2.0 and 2.5 mm/sec) had only resulted in the attainment of defective joints. It reveals that the employed 1.5mm/sec tool traverse speed have permitted the threaded cylindrically tapered pin geometry of the tool and its shoulder to soften the inner and exterior regions of the parent metals for a sufficient time, thereby, leading to the attainment of remarkable quality joints of distinctive alloys of Mg^{16,35,42,43}.

3.5. Interpretations from tensile fractography

With the objective of finding out the quality of the fabricated distinctive AZ31B and AZ91C joints of alloys of Mg, specimens for the tensile test were extracted from

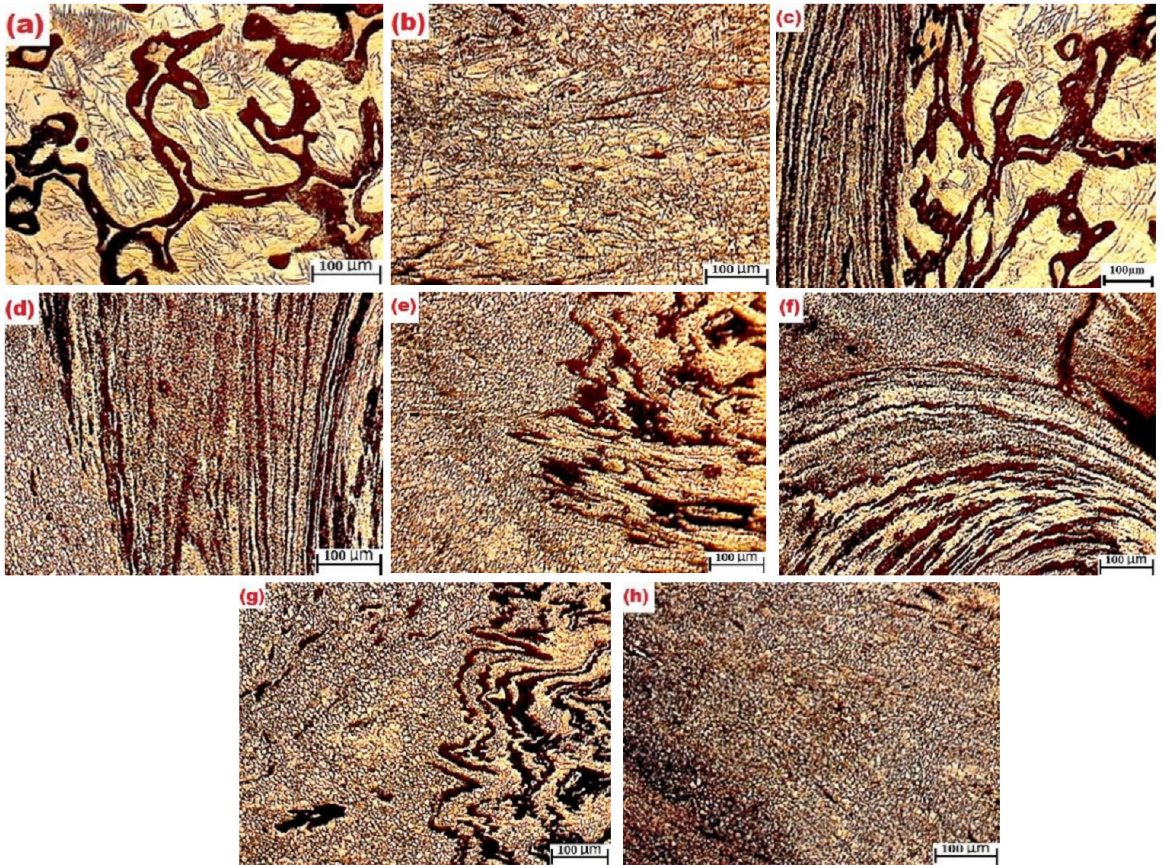


Figure 4. Micro-structural images of the parent metal (a) AZ91C (b) AZ31B and (c) – (h) various regions of the distinctive AZ31B-AZ91C joint of alloy of Mg fabricated at 1.5 mm/sec.

Flaw free joint no: II-3 and were subjected to tensile tests as per E8M-04 standards prescribed by American society for testing & materials^{44,45} and the diagrammatic representation of the size of the sample being extracted for performing tensile test is illustrated in the Figure 6.

Tensile strength exhibited by the joints fabricated during 2nd set of experimentation under varying speeds of traverse is graphically portrayed in the Figure 7. it can be noticed that, the flaw free joint No:II-3 fabricated at speed of traverse of 1.5 mm/sec have exhibited the highest value of strength (i.e., 186 MPa) when compared with other joints.

Tensile strength of 186 MPa was exhibited by the joint (Joint no: II-3) fabricated during the employment of speed of traverse of 1.5mm/sec. Figure 8 graphically compares the mechanical properties of the joint no: II-3 and both the parent metals (namely AZ31B and AZ91C).

By observing this graph, we can understand that, the tensile strength exhibited by the flaw-free joint (joint no:II-3) fabricated under the employment of speed of tool traverse of 1.5 mm/sec is nearly 78.81% of the parent metal namely AZ91C and nearly 70.72% of another parent metal namely AZ31B, which can be acknowledged as an acceptable value of strength for the scenario of distinctive joints^{16,28,46}.

In addition to this, the values of hardness were measured across the region of weld for the joints fabricated under the

2nd set of experimentation and their corresponding hardness values are graphically illustrated in the Figure 9. From this Figure 9, this it can be visualized that, the larger the size of the grains, lesser is the value of the hardness. Likewise, the reduction in the size of the grains have contributed for the improvement in the value of hardness of the joint, especially for the joint No:II-3, which inherits fine sized grains in their zone of nugget. The highest value of tensile strength was also exhibited by this Joint No:II-3, which helps us to understand that, the smaller is the size of the grains, higher is the value of their hardness and occurrence of fine sized grains in the zone of nugget will enhance the mechanical properties of the joints, as seen in the case of the Joint No:II-3.

With the objective of gaining more knowledge on the mechanism by which this flaw-free joint had encountered fracture during the tensile test, the fractured joint no:II-3 was subjected to analysis by scanning electron microscope (SEM) and the attained SEM images are portrayed in Figure 9a-c.

Slightly layered surfaces (flat surfaces) are clearly visible in all these fractured surface images, i.e., Figure 9a-c, which is a clear implication of the involvement of the brittle mode of mechanism of fracture. At the same time, characteristics relevant to ductile mode of fracture mechanism including micro voids can also be observed in Figure 9c. However, layered surfaces can be observed to occupy the majority areas

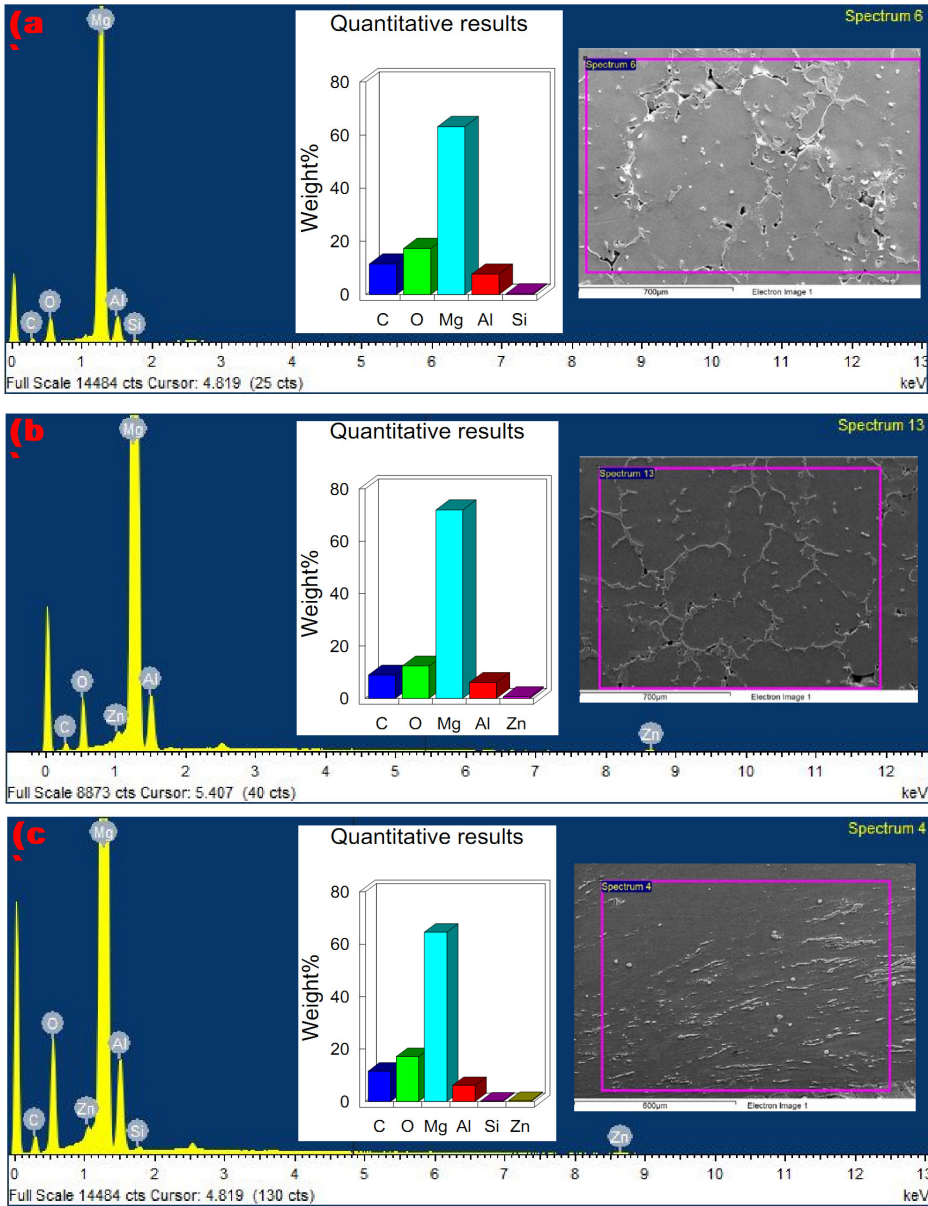


Figure 5. Energy dispersive X-ray analysis (EDAX) images and constituent element graphs of the parent metals namely (a) AZ91C; (b) AZ31B and (c) at the zone of nugget of the Joint no: II-3.

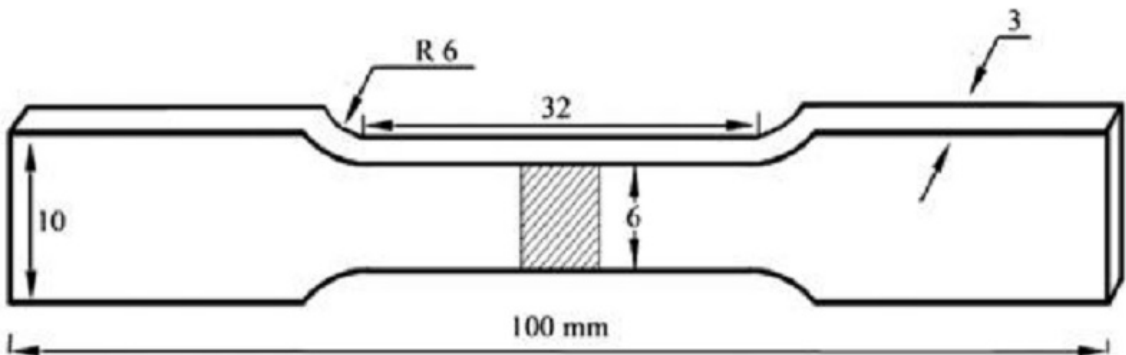


Figure 6. Diagrammatic representation of the size of the sample being extracted for tensile related test.

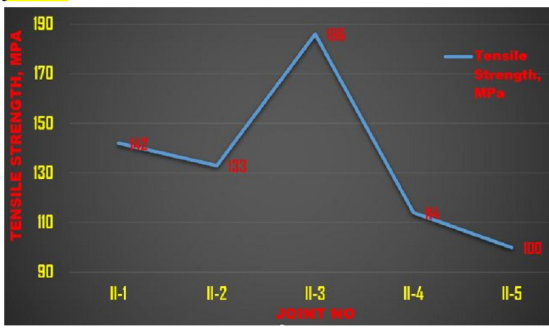


Figure 7. Graphical illustration of the tensile strength exhibited by joints fabricated under 2nd set of experimentation.

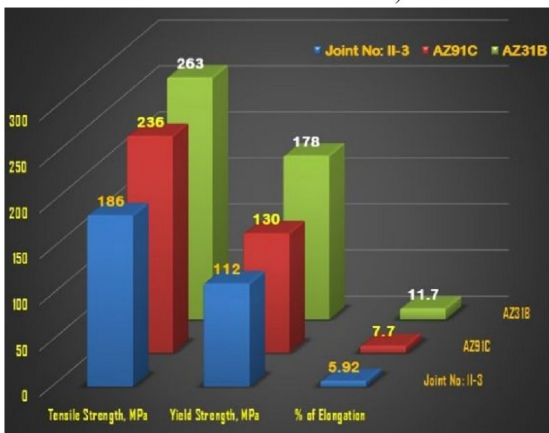


Figure 8. Graphical comparison of the mechanical properties of the joint no: II-3 and the parent metals i.e., AZ91C and AZ31B respectively.

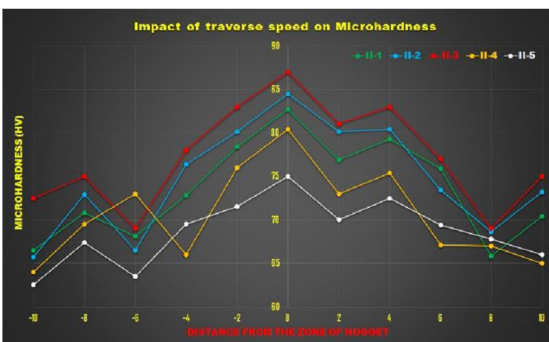


Figure 9. Graphical Illustration of the values of hardness measured across the region of weld for the joints fabricated under the 2nd set of experimentation.

of the fractured surfaces and the micro voids are present only in few portions, which declare that, in the fractured specimen, the brittle mode of mechanism of fracture was preeminent over the ductile mode of fracture mechanism^{4,40,47}.

In addition to this, we can also understand that, the initial points of commencement of fracture are those micro voids, which are visible clearly in Figure 9c. Major reasons

for these imperfections would have been associated with the generation of the brittle intermetallic phased constituents. The existence of Intermetallic phased constituents, namely, $Mg_{17}Al_{12}$ at these regions would have contributed to the supplementary brittleness in the zone of nugget and this would have reduced the tensile strength of the II-3 joint, when compared with that of the parent metals⁴⁸.

4. Conclusions

This investigation was conducted to gain more insight into the role of several parameters including tool pin geometry, speed of tool traverse, offset distance of tool etc during the joining of two distinctive alloys of Mg namely AZ31B and AZ91C by friction stir welding. Completely 2 unique sets of investigation were carried out using tools with two unlike geometries namely cylindrically tapered pin and threaded cylindrically tapered pin geometries. Outcomes deduced through this investigational work are enumerated below:-

- Macro-structures of the joints designated as I-1, I-2, I-4 and I-5 fabricated during 1st set by keeping offset distance of tool pin either 0.5 to 1mm towards AZ31B side or AZ91C side, possessed large-sized voids at their root portion.
- Macro-structure of the I-3 joint possessed negligible sized voids, announced that, tool pin offset distance should be maintained at 0mm for attaining flaw-free distinctive AZ31B and AZ91C joints.
- Joints (namely II-1, II-2, II-4 and II-5) fabricated during 2nd set of investigation employing threaded cylindrically tapered pin possessed defects including pores, cavities, voids etc. The intensities of these defects increased with the employment of higher speeds of tool travel (namely 2.0 mm/sec and 2.5 mm/sec).
- Flaw free joint no:II-3 announced that, the threaded cylindrically tapered pin geometry, tool's shoulder diameter (15mm) and ideal traverse speed (1.5 mm/sec) have jointly generated sufficient volume of heat and performed the function of enabling the mixture of constituents of the distinctive parent metals from root portion to crest portion in an enhanced manner.
- A tensile strength of 186 MPa was exhibited the flaw-free joint (Joint no: II-3) fabricated during the employment of threaded cylindrically tapered pin at a speed of traverse of 1.5mm/sec, tool offset distance of 0mm. This exhibited tensile strength is nearly 78.81% of the parent metal namely AZ91C and nearly 70.72% of another parent metal namely AZ31B.
- Existence of layered surfaces (in the tensile fractured specimen) over the majority areas of the fractured surfaces and the presence of micro voids in few portions, declared that, in the fractured specimen, the brittle mode of mechanism of fracture was preeminent over the ductile mode of fracture mechanism.

5. References

1. Shehabeldeen TA, Zhou J, Shen X, Yin Y, Ji X. Comparison of RSM with ANFIS in predicting tensile strength of dissimilar

- friction stir welded AA2024-AA5083 aluminium alloys. *Procedia Manufacturing*. 2019;37:555-62.
2. Santini FF, Plaine AH, Afonso CRM, Bergmann L, de Alcântara NG, dos Santos JF, et al. Microstructure features and mechanical properties of double-sided friction stir welded joints of AA2050-T84 thick plates. *Mater Res*. 2020;23(6):e20200309.
 3. Memon S, Paidar M, Mehta KP, Babaei B, Lankarani HM. Friction spot extrusion welding on dissimilar materials AA2024-T3 to AA5754-O: effect of shoulder plunge depth. *J Mater Eng Perform*. 2021;30(1):334-45.
 4. Nia AA, Shirazi A. Effects of different friction stir welding conditions on the microstructure and mechanical properties of copper plates. *Int J Miner Metall Mater*. 2016;23(7):799-809.
 5. Muthu Krishnan M, Maniraj J, Deepak R, Anganan K. Prediction of optimum welding parameters for FSW of aluminium alloys AA6063 and A319 using RSM and ANN. *Materials Today: Proceedings*. 2018;5(1):716-23.
 6. Mahgoub A, Bazoune A, Merah N, Al-Badour F, Shuaib A. Effect of welding parameters on the mechanical and metallurgical properties of friction stir spot welding of copper lap joint. *Arab J Sci Eng*. 2019;44(2):1283-92.
 7. Liu P, Sun S, Hu J. Effect of laser shock peening on the microstructure and corrosion resistance in the surface of weld nugget zone and heat-affected zone of FSW joints of 7050 Al alloy. *Opt Laser Technol*. 2019;112:1-7.
 8. Gharavi F, Ebrahimzadeh I, Amini K, Sadeghi B, Dariya P. Effect of welding heat input on the microstructure and mechanical properties of dissimilar friction stir-welded copper/brass lap joint. *Mater Res*. 2019;22(4):e20180506.
 9. Memon S, Paidar M, Ojo OO, Cooke K, Babaei B, Masoumehzad M. The role of stirring time on the metallurgical and mechanical properties during modified friction stir clinching of AA6061-T6 and AA7075-T6 sheets. *Results in Physics*. 2020;19:103364.
 10. Fernandes CA, Urtiga Filho SL, Suhuddin U, Santos JF. Effects of geometrical feature on microstructures and mechanical properties of refill friction stir spot welding 6061 aluminum alloy. *Mater Res*. 2019;22(6):e20190386.
 11. Singh K, Singh G, Singh H. Review on friction stir welding of magnesium alloys. *Journal of Magnesium and Alloys*. 2018;6(4):399-416.
 12. Mironov S, Sato YS, Kokawa H. Influence of welding temperature on material flow during friction stir welding of AZ31 magnesium alloy. *Metall Mater Trans, A Phys Metall Mater Sci*. 2019;50(6):2798-806.
 13. Hossein Baghdadi A, Fazilah Mohamad Selamat N, Sajuri Z, Hossein Kokabi A. Effect of travel speed on quality and welding efficiency of friction stir welded AZ31B magnesium alloy. *IACSIT Int J Eng Technol*. 2018;7(3):94-9.
 14. Hasan AF. CFD modelling of friction stir welding (FSW) process of AZ31 magnesium alloy using volume of fluid method. *Journal of Materials Research and Technology*. 2019;8(2):1819-27.
 15. Rajendran C, Abdulriyazdeen A, Abishek S, Aatheeshwaran A, Akash A. Prediction of relationship between angular velocity to the pitch line velocity (ω/v) on tensile strength of friction stir welded AA2014-T6 aluminium alloy joints: angular velocity to pitch line velocity ratio on FSW joints. *Forces in Mechanics*. 2021;4:100036.
 16. Rafiei R, Shamanian M, Fathi M, Khodabakhshi F. Dissimilar friction-stir lap-welding of aluminum-magnesium (AA5052) and aluminum-copper (AA2024) alloys: microstructural evolution and mechanical properties. *Int J Adv Manuf Technol*. 2018;94(9-12):3713-30.
 17. Argesi FB, Shamsipur A, Mirsalehi SE. Preparation of bimetallic nano-composite by dissimilar friction stir welding of copper to aluminum alloy. *Trans Nonferrous Met Soc China*. 2021;31(5):1363-80.
 18. Wang X, Morisada Y, Fujii H. Interface development and microstructure evolution during double-sided friction stir spot welding of magnesium alloy by adjustable probes and their effects on mechanical properties of the joint. *J Mater Process Technol*. 2021;294:117104.
 19. Tabasi M, Farahani M, Givi MKB, Farzami M, Moharami A. Dissimilar friction stir welding of 7075 aluminum alloy to AZ31 magnesium alloy using SiC nanoparticles. *Int J Adv Manuf Technol*. 2016;86(1-4):705-15.
 20. Dhanesh Babu SD, Sevvil P, Senthil Kumar R. Simulation of heat transfer and analysis of impact of tool pin geometry and tool speed during friction stir welding of AZ80A Mg alloy plates. *J Mech Sci Technol*. 2020;34(10):4239-50.
 21. Gopala Krishna G, Mahender T. Improving friction stir weldments joint efficiency of Aluminium AA6351 alloy by using coating technique. *Materials Today: Proceedings*. 2019;19(2):798-802.
 22. Osman N, Sajuri Z, Baghdadi AH, Omar MZ. Effect of process parameters on interfacial bonding properties of aluminium-copper clad sheet processed by multi-pass friction stir-welding technique. *Metals (Basel)*. 2019;9(11):1159.
 23. Selamat, N., Baghdadi, A., Sajuri, Z., Junaidi, S., Kokabi, A. Rolling effect on dissimilar friction stir welded aa5083-aa6061 aluminium alloy joints. *J Adv Manuf Technol*. 2020;14;2(1):49-61.
 24. Kumar PS, Chander MS. Effect of tool pin geometry on FSW dissimilar aluminum alloys - (AA5083 & AA6061). *Materials Today: Proceedings*. 2021;39(1):472-7.
 25. Rajendran C, Srinivasan K, Balasubramanian V, Balaji H, Selvaraj P. Effect of tool tilt angle on strength and microstructural characteristics of friction stir welded lap joints of AA2014-T6 aluminum alloy. *Trans Nonferrous Met Soc China*. 2019;29(9):1824-35.
 26. Sathish T, Sevvil P, Sudharsan P, Vijayan V. Investigation and optimization of laser welding process parameters for AA7068 aluminium alloy butt joint. *Materials Today: Proceedings*. 2021;37(2):1672-7.
 27. Baghdadi AH, Sajuri Z, Omar MZ, Rajabi A. Friction stir welding parameters: impact of abnormal grain growth during post-weld heat treatment on mechanical properties of Al-Mg-Si welded joints. *Metals (Basel)*. 2020;10(12):1607.
 28. Sajuri Z, Mohamad Selamat NF, Baghdadi AH, Rajabi A, Omar MZ, Kokabi AH, et al. Cold-rolling strain hardening effect on the microstructure, serration-flow behaviour and dislocation density of friction stir welded AA5083. *Metals (Basel)*. 2020;10(1):70.
 29. Eskandari M, Jamshidi Aval H, Jamaati R. The study of thermomechanical and microstructural issues in dissimilar FSW of AA6061 wrought and A390 cast alloys. *J Manuf Process*. 2019;41:168-76.
 30. Patel N, Bhatt KD, Mehta V. Influence of tool pin profile and welding parameter on tensile strength of magnesium alloy AZ91 during FSW. *Procedia Technol*. 2016;23:558-65.
 31. Wang W, Han P, Qiao K, Li T, Wang K, Cai J, et al. Effect of the rotation rate on the low-cycle fatigue behavior of friction-stir welded AZ31 magnesium alloy. *Eng Fract Mech*. 2020;228:106925.
 32. Asl NS, Mirsalehi SE, Dehghani K. Effect of TiO₂ nanoparticles addition on microstructure and mechanical properties of dissimilar friction stir welded AA6063-T4 aluminum alloy and AZ31B-O magnesium alloy. *J Manuf Process*. 2019;38:338-54.
 33. Md S, Birru AK. Mechanical and metallurgical properties of friction stir welded dissimilar joints of AZ91 magnesium alloy and AA 6082-T6 aluminium alloy. *J Magnes Alloy*. 2019;7(2):264-71.
 34. Sevvil P., Dhanesh Babu S.D., Senthil Kumar R. Peak temperature correlation and temperature distribution during joining of AZ80A Mg alloy by FSW – a numerical and experimental investigation. *J Mech Eng*. 2020;66(6):395-407.
 35. Choi J-W, Liu H, Ushioda K, Fujii H. Dissimilar friction stir welding of immiscible titanium and magnesium. *Materialia*. 2019;7:100389.

36. Baghdadi AH, Mohamad Selamat NF, Sajuri Z. Effect of tool offsetting on microstructure and mechanical properties dissimilar friction stir welded Mg-Al alloys. *IOP Conf Series Mater Sci Eng.* 2017;238(1):012018.
37. Fu B, Shen J, Suhuddin UFHR, Pereira AAC, Maawad E, dos Santos JF, et al. Revealing joining mechanism in refill friction stir spot welding of AZ31 magnesium alloy to galvanized DP600 steel. *Mater Des.* 2021;209:109997.
38. Meng Y, Ma Y, Chen S, Han Y, Chen S, Huang J, et al. Friction stir butt welding of magnesium alloy to steel by truncated cone-shaped stirring pin with threads. *J Mater Process Technol.* 2021;291:117038.
39. Wang T, Shukla S, Gwalani B, Komarasamy M, Reza-Nieto L, Mishra RS. Effect of reactive alloy elements on friction stir welded butt joints of metallurgically immiscible magnesium alloys and steel. *J Manuf Process.* 2019;39:138-45.
40. Baghdadi AH, Sajuri Z, Selamat NFM, Omar MZ, Miyashita Y, Kokabi AH. Effect of intermetallic compounds on the fracture behavior of dissimilar friction stir welding joints of Mg and Al alloys. *Int J Miner Metall Mater.* 2019;26(10):1285-98.
41. Dhanesh Babu SD, Sevvel P, Senthil Kumar R, Vijayan V, Subramani J. Development of thermo mechanical model for prediction of temperature diffusion in different FSW tool pin geometries during joining of AZ80A Mg alloys. *J Inorg Organomet Polym Mater.* 2021;31(7):3196-212.
42. Sangalli G, Lemos GVB, Martinazzi D, Lessa CRL, Beskow AB, Reguly A. Towards qualification of friction stir welding to AA5083-O and AA5052-O aluminum alloys. *Mater Res.* 2019;22(5):e20190349.
43. Mehta KP, Patel R, Vyas H, Memon S, Vilaça P. Repairing of exit-hole in dissimilar al-mg friction stir welding: process and microstructural pattern. *Manuf Lett.* 2020;23:67-70.
44. Elangovan K, Balasubramanian V, Babu S. Developing an empirical relationship to predict tensile strength of friction stir welded AA2219 aluminum alloy. *J Mater Eng Perform.* 2008;17(6):820-30.
45. Motalleb-nejad P, Saeid T, Heidarzadeh A, Darzi K, Ashjari M. Effect of tool pin profile on microstructure and mechanical properties of friction stir welded AZ31B magnesium alloy. *Mater Des.* 2014;59:221-6.
46. Cintra JP Fo, Araújo L Fo, Itikava RK, Silva MM, Perez RA. Thermomechanical modelling of FSW process using a cylindrical tool in an aluminum alloy Alclad AA 2024-T3. *Mater Res.* 2018;21(4):e20170773.
47. Sathesh C, Sevvel P, Senthil Kumar R. Experimental identification of optimized process parameters for FSW of AZ91C Mg alloy using quadratic regression models. *J Mech Eng.* 2020;66:736-51.
48. Wiedenhoft AG, Amorim HJ, Rosendo TS, Tier MAD, Reguly A. Effect of Heat Input on the Mechanical Behaviour of Al-Cu FSW Lap Joints. *Mater Res.* 2018;21(4):e20170983.